frontiers | Frontiers in Physics

TYPE Original Research
PUBLISHED 20 October 2025
DOI 10.3389/fphy.2025.1694078

OPEN ACCESS

EDITED BY
Edward John Sambriski,
Delaware Valley University, United States

REVIEWED BY
Saravana Prakash Thirumuruganandham,
SIT Health, Quito, Ecuador
Segun Oke,
Alabama A & M University, United States

*CORRESPONDENCE
A. A. Coreno-Cortés,
acoreno@pceim.unam.mx
I. Santamaría-Holek,
isholek.fc@gmail.com

RECEIVED 27 August 2025
ACCEPTED 06 October 2025
PUBLISHED 20 October 2025

CITATION
Coreno-Cortés AA, Cortés-Cuán MA and Santamaría-Holek I (2025) PLGA–PEG–PLGA self-aggregation study via fragment dissipative particle dynamics and quantum determined interaction parameters. *Front. Phys.* 13:1694078. doi: 10.3389/fphy.2025.1694078

PLGA–PEG–PLGA self-aggregation study via fragment dissipative particle dynamics and quantum determined interaction parameters

A. A. Coreno-Cortés*, M. A. Cortés-Cuán and I. Santamaría-Holek*

UMDI-Facultad de Ciencias, Universidad Nacional Autónoma de México Campus Juriquilla, Querétaro, México

In this work, we used Conductor-like Screening Model for Real Solvents (COSMO-RS) to calculate the parameters that characterize the interactions between molecular segments in a coarse-grained representation of the PLGA–PEG–PLGA mesomolecule. The computed activity coefficients at infinite dilution were then used to obtain the thermodynamic Flory–Huggins interaction parameters, which were subsequently transferred to Dissipative Particle Dynamics simulations. In these simulations, beads interact through repulsive conservative parameters to investigate the self-aggregation of the PLGA–PEG–PLGA triblock copolymer. The parameters were then applied in Dissipative Particle Dynamics (DPD) simulations at varying copolymer concentrations. Self assembling at different concentrations was studied. Transitions from core-shell spherical micelles to onion-like, columnar and lamellar structures were obtained in terms of copolymer concentration, setting the optimal concentration range for different drug loaded vehicles.

KEYWORDS

self-assembly, activity coefficients, flory-huggins, first principles, dissipative particle dynamics

1 Introduction

Polymeric micelles formed from amphiphilic block copolymers in aqueous solution have been extensively studied in recent decades as drug delivery systems Cabral et al. [1], Hossen et al. [2]. They offer high *in vivo* stability, efficient drug loading, good biocompatibility, and effective targeted drug release. These properties contribute to enhanced chemotherapeutic efficacy and reduced drug toxicity, Fukushima [3], Liao et al. [4], Zhang et al. [5]. Although polymeric micelles have attracted considerable interest as drug carriers, a comprehensive understanding of their structures and morphologies upon drug loading remains limited.

Various polymeric micelles can serve as drug delivery vehicles; among them, PLGA-b-PEG-b-PLGA micelles—composed of poly (lactic acid-co-glycolic acid)-b-poly (ethylene

glycol)-b-poly (lactic acid-co-glycolic acid)—have garnered significant attention, Zhang et al. [6], Yan et al. [7]. The PLGA-b-PEG-b-PLGA copolymers materials have advantages such as biocompatibility, degradability, thermosensitivity and controlled release, Yu et al. [8]. The capacity of PLGA-b-PEG-b-PLGA micelles to solubilize hydrophobic drugs stems from their core–shell structure, Chen et al. [9]. Extensive studies have been conducted on their drug-loading capabilities, for example, it has been showed that PLGA-b-PEG-b-PLGA can carry doxorubicin (DOX) drugs, Wang et al. [10], in this study they found that due to the molecular interactions between hydrophobic blocks, PLGA-b-PEG-b-PLGA have exhibited long lasting maintenance after subcutaneous injection *in vivo*, Chang et al. [11]. Khorshid et al. [12] explored the influence of hydrophylic PEG block length keeping the hydrophobic PLGA blocks constant. They observed that, as the temperature varied, the aggregate structure transitioned from spherical core–shell micelles to cylindrical micelles and eventually to packed cylindrical arrangements.

Since experimental techniques alone have limitations in revealing the detailed molecular distribution and dynamic behavior of drug-loaded systems, computational simulations have been widely employed to study drug encapsulation and release mechanisms. Among computational approaches, dissipative particle dynamics (DPD) has shown to be an efficient mesoscopic simulation method, well-suited for studying complex multiphase systems. It has been successfully used to investigate the formation, drug distribution, and release processes in drug-loaded micelles, Hoogerbrugge and Koelman [13]. DPD is a coarse-grained simulation method used to study surfactant aggregation in solution over extended timescales. In this mesoscopic approach, molecules are represented as beads, allowing for efficient modeling of self-assembly processes. Beyond surfactants, DPD has also been applied to explore more complex liquid systems, Groot and Rabone [14]. Yang et al. [15] used DPD simulations to investigate comicellization behavior, drug distribution patterns, and dual pH/reduction-responsive drug release in mixed micelles. Similarly, Kuru et al. employed coarse-grained DPD simulations to study the morphology, drug encapsulation, and release characteristics of PEG–PLA–PEG amphiphilic block copolymer systems. In more recent years Wang et al. [10] used DPD to study the morphologies and structures of the PLGA-b-PEG-b-PLGA influenced by the copolymer concentration and composition. The structures reported were micelles observed as spherical, onionlike, columnar, and lamellar structures.

Several coarse-grained computational approaches have been reported for simulating these types of dynamics, Cooke et al. [16], Cooke and Deserno [17]. Typically, these models are parameterized using inverse Monte Carlo techniques based on atomistic simulations, Elezgaray and Laguerre [18], Shelley et al. [19]. However, such parameterizations present limitations particularly regarding temperature, which is constrained to the range used during calibration. For example, the widely used MARTINI force field is valid only between 270 and 330 K, Marrink et al. [20]; simulations beyond this range may yield inaccurate results. Another significant limitation lies in modeling interactions between polar compounds, where the forces are often underestimated.

Nivón-Ramírez et al. [21] used a methodology to estimate coarse-grained repulsion parameters a_{ij} using quantum chemistry calculations. For the rapid generation of phase equilibrium data—relevant in applications such as process simulations—simplified numerical models like equations of state (EOS) or excess Gibbs free energy (g^E) formulations are typically employed, Shimoyama and Iwai [22]. Among them, COSMO-type g^E models and the Peng–Robinson (PR) EOS are widely used to describe the phase behavior of multicomponent mixtures.Grensemann and Gmehling [23] demonstrated that COSMO-based models can predict fluid-phase coexistence with high reliability, even for systems lacking experimental parameters, Merker et al. [24]. In this context, comparing the predictive performance of these approaches is essential to validate coarse-grained interaction parameters obtained from quantum-chemical methods.

Solvent effects are incorporated through the Conductor-like Screening Model (COSMO) and the COSMO-Real Solvent (COSMO-RS) model, which allow for the computation of chemical potentials (μ_{ij}) for species i and j in a pure solvent or mixture. From these values, activity coefficients (γ_{ij}) are derived and used to calculate the Flory-Huggins interaction parameter (χ_{ij}).According to Groot and Warren, a linear relationship connects χ_{ij} to the mesoscopic parameter a_{ij} via $a_{ij} = 25 + 3.5\chi_{ij}^{\infty}$ Since χ_{ij}^{∞} is temperature-dependent, so is a_{ij}. This approach enables the modeling of molecular interactions without the need for empirical force field parameterization, and it is applicable to any chemical species.

COSMO-type models do not rely on tabulated parameters, as they only require quantum mechanical solvation calculations as input to predict phase equilibria. Consequently, they are not limited by missing parameter values and can be applied to a broader range of chemical species. This is particularly valuable in industrial settings, where new or poorly characterized compounds are often of interest [25].

In this study, the interaction parameters of the PLGA-b-PEG-b-PLGA copolymer were validated through a modified COSMO-RS methodology at 298.15 K. These parameters were subsequently employed in Dissipative Particle Dynamics (DPD) simulations to examine the influence of copolymer concentration on the self-assembly of unloaded (blank) structures. The article is organized as follows: in Section 2 we present the DPD methodology with the COSMO-RS method, in Section 3 we display our findings using first principle and mesoscopic techniques and finally in Section 4 we provide an insight from our work.

2 Materials and methods

2.1 Dissipative particle dynamics

DPD simulations are based on Newton's equations of motion and aim to represent fluid behavior and interactions as simply as possible at the mesoscopic scale, minimizing computational cost. The core idea is to model interactions using a pairwise repulsion parameter a_{ij}, while preserving the essential physico-chemical characteristics of the system. The DPD model represents point-like particles that interact through defined force sets. Physically, each mesomolecule is composed of a group of beads that move coherently and are

connected by harmonic springs Groot and Warren [26], Groot and Rabone [14].

DPD is a coarse-grained molecular dynamics method in which the system's time evolution is governed by the equations of motion, that is $\frac{d\mathbf{p}_i(t)}{dt} = \mathbf{f}_i(t)$, where $\mathbf{p}_i$ is the momentum of the bead i and $\mathbf{f}_i(t)$ is the total force acting on it.

The value of the force $\mathbf{F}$ applied to the DPD particles i and j separated a distance r_{ij}, has three contributions as defined in Equation 1, a conservative force ($\boldsymbol{F}_{\boldsymbol{ij}}^{\boldsymbol{C}}$) which is related to the chemical nature of the DPD particles (as shown in Equation 2), a dissipative force ($\boldsymbol{F}_{\boldsymbol{ij}}^{\boldsymbol{D}}$) that models the friction between particles related to viscosity as described in Equation 3 and a random force $\boldsymbol{F}_{\boldsymbol{ij}}^{\boldsymbol{R}}$ that imitates accounts for thermal fluctuations:

$$\boldsymbol{F}_{\boldsymbol{i}} = \sum_{j \neq i} \boldsymbol{F}^{\boldsymbol{C}} + \boldsymbol{F}^{\boldsymbol{D}} + \boldsymbol{F}^{\boldsymbol{R}}, \tag{1}$$

Where,

$$\boldsymbol{F}_{\boldsymbol{ij}}^{\boldsymbol{C}} = -a_{ij} w^{c}\left(r_{ij}\right) \widehat{\boldsymbol{r}_{\boldsymbol{ij}}}, \tag{2}$$

$$\boldsymbol{F}_{ij}^{D} = -\gamma w^{D}\left(r_{ij}\right)\left(\hat{\boldsymbol{r}}_{\boldsymbol{ij}} \cdot \boldsymbol{v}_{\boldsymbol{ij}}\right)\hat{\boldsymbol{r}}_{\boldsymbol{ij}}, \tag{3}$$

$$\boldsymbol{F}_{ij}^{R} = \sigma w^{R}\left(r_{ij}\right)\hat{r}_{ij}\zeta_{ij}/\sqrt{\delta t}. \tag{4}$$

All forces act within a cutoff distance r_c; if the separation between particles i and j exceeds r_c ($r_{ij} > r_c$), the force becomes zero. All beads are assumed to have an effective diameter equal to r_c, which is set as the unit length. The term ζ in Equation 4 is a Gaussian random variable with zero mean and unit variance. The functions $w^{c}(r_{ij}), w^{D}(r_{ij})$ and $w^{R}(r_{ij})$ are weight functions corresponding to the conservative, dissipative, and random forces, respectively. The parameter a_{ij} defines the strength of the conservative force $\boldsymbol{F}_{\boldsymbol{ij}}^{\boldsymbol{C}}$ and governs the thermodynamic behavior of the DPD fluid. Meanwhile, γ and σ denote the amplitudes of the dissipative and random (noise) forces, respectively.

To determine the interaction parameters (a_{ij}), we adopted the approach proposed by Groot [27] as a foundation, refining it through quantum mechanical calculations based on the Conductor-like Screening Model (COSMO) and Conductor-like Screening Model Real Solvents (COSMO-RS), with additional corrections to account for temperature effects, Oviedo-Roa et al. [28]; Nivón-Ramírez et al. [29]; Alasiri and Chapman [30]; Saathoff [31].

2.2 Scaling from atomistic models to mesoscopic representations

In the coarse-graining process employed for DPD modeling, all beads are assumed to occupy the same volume (V_{bead}), irrespective of their chemical identity Maiti and McGrother [32]; Rajkamal and Vedantam [33]. The PLGA-b-PEG-b-PLGA copolymer was modeled according to the scheme proposed by Wang et al. [34], as illustrated in Figure 1. In this representation, the polymer is segmented into three components: lactic acid (L) and glycolic acid (G), which form the hydrophobic PLGA blocks, and polyethylene glycol (PEG), which constitutes the central hydrophilic segment. This amphiphilic configuration promotes micelle or nanoparticle formation in aqueous environments Lee et al. [35].

To determine the volume of each bead (V_{bead}), we used Equation 5:

$$V_{\text{bead}} = \frac{V_{\text{molecule}}}{\lambda}, \tag{5}$$

where λ denotes the number of fragments into which the solute molecule is divided ($\lambda = 5$), and V_{molecule} is the molecular volume obtained from quantum-mechanical geometry optimizations. The choice of $\lambda = 5$ was selected to ensure that the bead volume closely approximated the molecular volume, minimizing deviations, while also preserving the distinctive characteristics of the hydrophilic and hydrophobic blocks in the copolymer.

The number of water molecules in one bead is calculated by Equation 6:

$$N_{\text{water}} = \frac{V_{\text{bead}}}{V_{\text{water}}}, \tag{6}$$

where V_{water} is the volume of a single water molecule. In these simulations, all beads are assumed to have the same mass, equivalent to the combined mass of the N_{water} solvent molecules contained in a water bead. For this work, $N_{\text{water}} = 2.75$. In practice, it is rounded to three to simplify the model, as illustrated in Figure 1C.

Molecular volume calculations for the solute the molecule and incorporate a continuous approximation of the solvent environment via the conductor-like screening model (COSMO), Klamt and Eckert [36]; Klamt [37]. In order to maintain consistency with the atomistic-quantum calculations of the Flory–Huggins parameter, χ_{ij}, COSMO was used throughout.

The infinite-dilution activity coefficient, γ_{ij}^{∞}, was obtained in natural logarithmic form at room temperature. With γ_{ij}^{∞} in hand, the Flory–Huggins thermodynamic interaction parameter, χ_{ij}^{∞}, is derived using the liquid lattice model:

$$\chi_{ij}^{\infty} = \lim_{\phi_j \to 1} \chi_{ij} = \ln\left(\gamma_{ij}^{\infty}\right) + \ln\left(\nu_{ij}\right) - \left(1 - \frac{1}{\nu_{ij}}\right), \tag{7}$$

where $\nu_{ij} = \frac{\nu_j}{\nu_i}$ is the ratio of molecular volumes between the solvent and solute fragments. To evaluate the infinite-dilution activity coefficients required in Equation 7, we employed COSMO with a statistical thermodynamic treatment founded on the surface charge distribution of the molecules, as shown in Equation 8:

$$\ln\left(\gamma_{ij}^{\infty}\right) = \frac{\mu_{ij}^{\text{PSEUDO}} - \mu_i^{P}}{RT}. \tag{8}$$

Next, the interaction parameters were determined through a geometry optimization of the PLGA-b-PEG-b-PLGA polymer using density functional theory (DFT) within the TURBOMOLE software suite, accessed through the TMoleX 2025 interface. The DFT calculations were conducted under the COSMO continuous solvation model, Klamt [38], with the def-TZVP (triple-zeta valence polarized) atomic basis set, Schäfer et al. [39,40] and the Becke-Perdew (BP) functional, specifically B88-VWN-P86, Ahlrichs et al. [41]. Both geometric optimization and self-consistent field (SCF) procedures were implemented with an energy convergence criterion of 10^{-9} Ha. Following optimization, energy calculations were performed on each neutral, segmented molecule using the same level of theory.

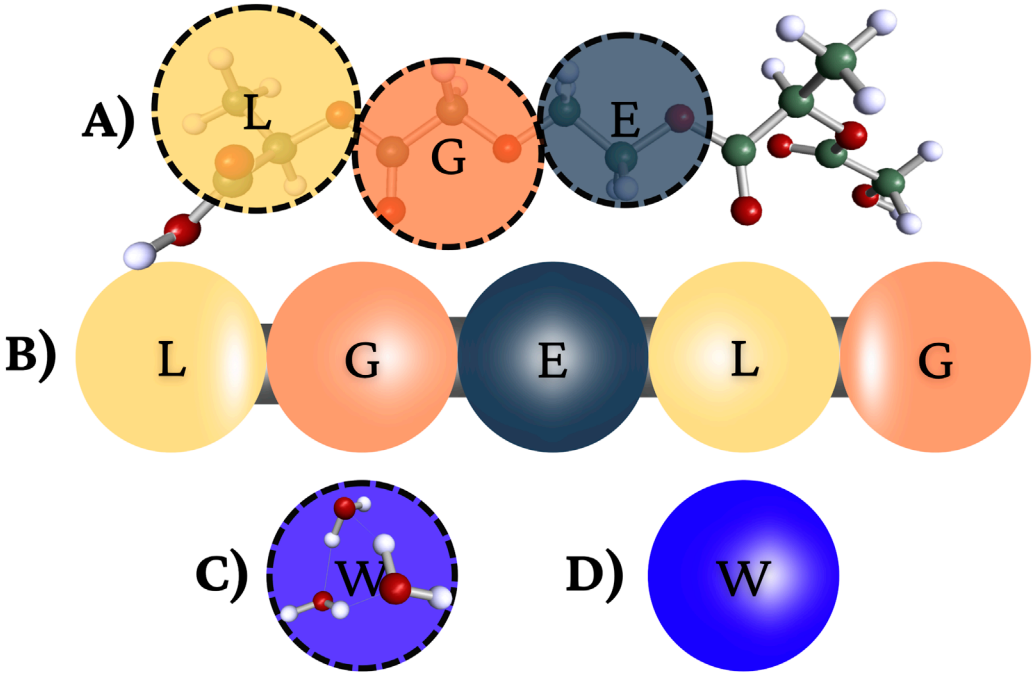

FIGURE 1
(A) Schematic representation of the PLGA-b-PEG-b-PLGA copolymer. The lactic acid (L) block is shown in yellow, the glycolic acid (G) block in flesh color, and the polyethylene glycol (E) segment in dark. **(B)** Coarse-grained DPD representation of the copolymer. **(C)** Atomistic snapshot of three water molecules (H_2O) corresponding to one coarse-grained water bead. **(D)** Coarse-grained DPD representation of a single water bead.

The liquid mixture was then modeled with COSMOthermX, Klamt and Schüürmann [42] under the COSMO-RS framework, effectively treating the molecules as if immersed in an ideal conductor. The parameter file BP_TZVP_C21_0111.ctd, Diedenhofen and Klamt [43], was selected to match the chosen basis set and level of theory.

In homogeneous systems, the interaction parameters for identical species simplify to $\nu_{ii} = 1$, $\ln(\gamma_{ii}^{\infty}) = 0$, and $\chi_{ii}^{\infty} = 0$, Nivón-Ramírez et al. [29], reflecting a uniform interaction within a single species. Consequently, the activity coefficient equals 1, and the corresponding repulsion coefficient is constant.

For identical molecules, the following DPD repulsion parameters follow, Xu et al. [44]:

$$a_{ii} = k_B T \frac{k^{-1} N_{\text{water}} - 1}{2\alpha\rho_{\text{DPD}}}, \tag{9}$$

where $k_B T$ represents the thermal energy (reduced to one at 298.15 K), and $k^{-1} = 15.9835$ is the dimensionless compressibility at this temperature. The term N_{water} is the number of water molecules contained in one coarse-grained bead, α is a proportionality constant (0.101 ±0.001) adjusting the relationship between the Flory–Huggins parameter and the DPD repulsion parameters, Groot and Warren [45], and $\rho_{\text{DPD}} = 3$ (in DPD units) is the chosen numerical density. It is important to note that the mapping scheme of three water molecules per bead ($N_{\text{water}} = 3$) establishes both the fragmentation and the bead volumes; adopting a different scheme would require a complete re-parameterization, including fragments, bead volumes, sigma profiles, activity coefficients, ν_{ij}, and a_{ij}.

According to Groot and Rabone (Equation 10) [46], for a system at $\rho_{\text{DPD}} = 3$:

$$\chi = 0.231 \pm 0.001\,\Delta a, \tag{10}$$

where $\Delta a = a_{ij} - a_{ii}$ is the excess repulsion between dissimilar particle types. Moreover, adopting a coarse-graining factor of $N_{\text{water}} \approx 3$ makes χ directly proportional to the bead size. Hence, when multiple elementary molecules are clustered into one bead, χ is scaled following:

$$\chi = N_{\text{water}} \chi_{ij}^{\infty}. \tag{11}$$

Because atomistic simulations work at the molecular scale, it becomes necessary to adjust χ to reflect the coarse-grained representation. Thus, if a water bead comprises roughly three water molecules, Maiti and McGrother [47], the solute–solvent interaction parameter is modified by:

$$a_{ij} = a_{ii} + \frac{N_{\text{water}} \chi_{ij}^{\infty}}{0.231}. \tag{12}$$

In Equation 12, a_{ij} is the repulsion parameter between beads, χ_{ij} is the Flory–Huggins parameter for components i and j, and $k_B T$ is taken as the energy unit in DPD. A reduced cutoff radius $r_c = 1$ is used, determined by $r_c = \sqrt{\rho_{\text{DPD}}\, V_{\text{bead}}}$. In this work, the cutoff radius (r_c) in real units is 6.28 Å, and each bead's effective diameter is approximately $0.86\, r_c$. With this convention, both r_c and $k_B T$ are set to one within the DPD framework, Khedr and Striolo [48].

TABLE 1 Molecular properties of polyethylene glycol (E), glycolic acid (G), lactic acid (L), and a reference system of three water molecules (W) at 298.15 K.

Molecule	Density (g/mL)	Volume Å^3	Atomic weight (g/mol)	Molar volume (cm^3/mol)
E	0.78	97.95	46.07	58.98
G	1.16	86.30	60.05	51.97
L	0.99	124.39	74.08	74.91
LGELG	1.30	413.06	322.27	248.75
W	1.00	30.00	18.02	18.07

TABLE 2 DPD interaction parameters between different structural units.

Bead *i* (solvent)	Bead *j* (solute)	v_{ij}	$\ln(Y_{ij}^{inf})$	X_{ij}^{inf}	a_{ij}
W	W	1.00	0.00	0.00	78.00
W	L	4.15	1.34	2.01	104.07
W	G	2.88	0.06	0.47	84.07
W	E	3.26	0.51	1.00	90.94
E	G	1.48	0.94	1.01	91.13
E	L	1.27	0.64	0.67	86.65
G	L	1.44	0.89	0.95	90.37

3 Results and discussion

3.1 Interaction parameters

Table 1 presents the molecular volumes at 298.15 K used for temperature correction. Based on these volumes, a bead volume of 82.61 Å^3 is obtained, corresponding to $N_{water} = 2.75$.

The ratios of molecular volumes employed to compute the solute–solvent interaction parameters are shown in Table 2, along with the corresponding DPD interaction parameters a_{ij}. The diagonal terms a_{ii} were taken as 78, in accordance with Equation 9.

Using Equation 11 and the volumetric coefficients v_{ij}, $\ln(Y_{ij}^{inf})$, and X_{ij}^{inf}, the values of a_{ij} were determined. Table 2 shows that the largest a_{ij} arises for the water (W)–lactic acid (L) combination, signifying a lower affinity between those two components. By contrast, ethylene glycol (E)–glycolic acid (G) exhibits a moderate a_{ij} (91.13), suggesting more compatibility. These distinctions in a_{ij} values are vital for explaining the solubility and mixture behavior in fluid dynamics simulations. They align with the observations by Merve et al. and Yildiz et al. Kuru et al. [49]; Yildiz and Kacar [50], though they differ from the values reported by Wang et al. Wang et al. [34]. Supplementary Figure S3 in the Supplementary Material illustrates the workflow of our methodology.

Through the COSMO method, the polarization charge density (SCD) is also obtained. Positive SCD values designate partially negative charge regions, whereas negative values correspond to regions of partial positive charge. The DFT-COSMO calculations generate a SCD distribution, which is transformed into sigma profiles (σ-profiles), Scheffczyk et al. [51]. Then, COSMO-RS uses these profiles to compute local contact energies and chemical potentials of mixture components, Klamt et al. [52].

Figure 2 displays the SCD profiles for water (W; magenta), lactic acid (L; blue), glycolic acid (G; green), and ethylene glycol (E; red). The x-axis corresponds to σ values, whereas the y-axis shows the distribution function $\rho(\sigma)$. Water presents two prominent peaks around 0.018 e/Å^2 and −0.016 e/Å^2, consistent with its well-known hydrogen-bonding capability Mullins et al. [53]. Lactic acid displays peaks at about −0.007 e/Å^2 and 0.010 e/Å^2, correlated with polar regions in its carboxyl group and less negative sites elsewhere. Glycolic acid has a strong negative peak at −0.008 e/Å^2, indicating a high capacity to accept hydrogen bonds, and a positive peak near 0.010 e/Å^2. Ethylene glycol shows a negative region around −0.002 e/Å^2, due to the oxygen atom in its structure and a maximum positive peak of about 0.014 e/Å^2 in its carbon backbone.

Based on these profiles, good miscibility is expected between water (W) and glycolic acid (G), as both exhibit pronounced negative σ peaks. Lactic acid (L) and ethylene glycol (E) can also interact favorably, albeit less strongly than W–G. Because all fragments are predominantly polar and capable of hydrogen bonding, they are generally miscible, with W–G showing the highest affinity. This conclusion is supported by the interaction parameters in Table 2 showed by the repulsion parameters.

3.2 Dissipative particle dynamics results

The DPD simulations are performed in a $20 \times 20 \times 20$ cubic box with periodic boundary conditions, these conditions were guided by standard practices in dissipative particle dynamics (DPD) simulations, where the simulation domain should be sufficiently large to accommodate the characteristic length scales of the self-assembled structures and minimize finite-size effects Groot and Warren [26], Al-Jabri and Rodgers [54]. We used DL_MESO, Seaton et al. [55]. It is worth mention that previous simulations have showned that this box is sufficient to avoid the finite-size effects, Guo et al. [56]. The simulations were carried out in the canonic ensamble (NVT). The simulation temperature used was $k_BT = 1$, we set the bead density to $\rho = 3$ with a fricction coefficient

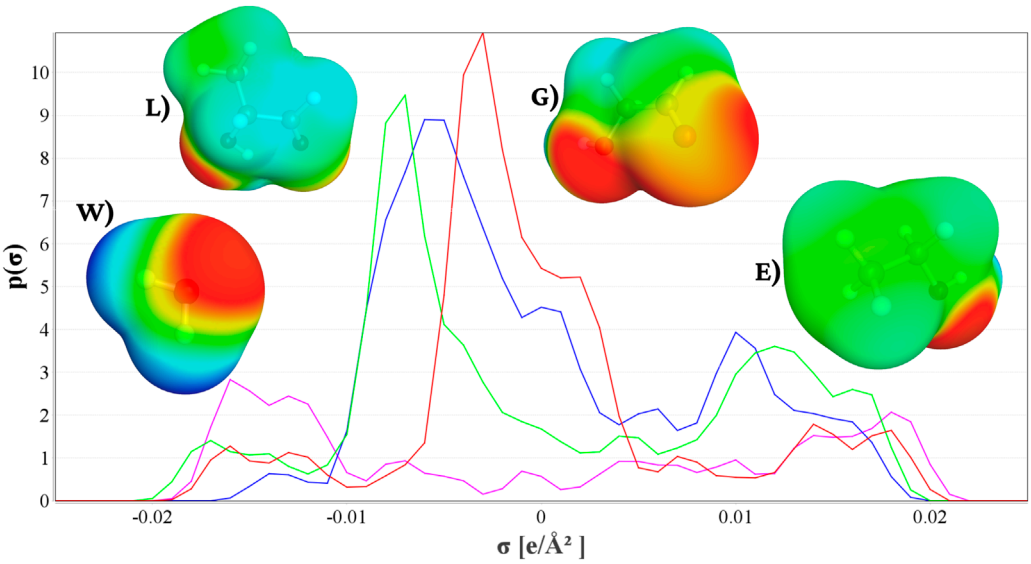

FIGURE 2
SCD profiles of each molecular fragment: (W) water (magenta line), (L) lactic acid (blue line), (G) glycolic acid (green line), and (E) ethylene glycol (red line).

$\gamma = 4.5$ and a cutoff radius $r_c = 1$. These conditions ensured the system relaxation. The initial configuration of the components was randomly placed in the simulation box. We run the simulation for 4×10^5 steps with a time step $\Delta t = 0.05$ to balance numerical stability with computational efficiency until thermodynamic equilibrium was achived.

We work with the PLGA-b-PEG-b-PLGA copolymer and water, the PLGA is the hydrophobic block, PEG is the hydrophilic block. Since we propose a more complete coarse grained model based on quantum calculations, we refer to the model in Figure 1 to represent the beads of the PLGA-b-PEG-b-PLGA copolymer and for water. As shown, several atoms or functional groups are represented as a DPD bead as we highlighted by color. We fragment the PLGA-b-PEG-b-PLGAThe in 5 parts: lactic acid (L) block shown in yellow, the glycolic acid (G) block in flesh color, and the polyethylene glycol (E) segment in dark. We represent three water molecules by one blue bead.

3.3 Morphologies and structures of the PLGA-b-PEG-b-PLGA micelles

The $PLGA_3$-b-PEG_7-b-$PLGA_3$ copolymer was selected to represent the real $PLGA_{1200}$-b-PEG_{1450}-b-$PLGA_{1200}$ copolymer, Wang et al. [10]. The PLGA-b-PEG-b-PLGA copolymers are theoretically predicted to form core–shell spherical micelles in aqueous environments, Yu et al. [57], Wang et al. [10]. To investigate the influence of PLGA-b-PEG-b-PLGA concentration c_{cp} on micelle morphologies and structures, DPD simulations were performed using $PLGA_3$-b-PEG_7-b-$PLGA_3$ concentrations ranging from 1.0% to 40%. It can be observed in Figure 3A that $PLGA_3$-b-PEG_7-b-$PLGA_3$ copolymers are capable of self-assembling into micelles in aqueous solution at a low copolymer concentration of $c_{cp} = 1.0\%$. The micellar microstructure exhibits significant variations as the concentration of $PLGA_3$-b-PEG_7-b-$PLGA_3$ copolymer increases from $c_{cp} = 1.0\%$ to 5%, the hydrophobic beads L, E form the hidrophobyc core of the micelle and the hydrophilic bead G sorrounds the block arrange. As the concentration of $PLGA_3$-b-PEG_7-b-$PLGA_3$ copolymer increases from $c_{cp} = 7.5\%$ to 15%, the structures packed and indicate onionlike structures, Guo et al. [58]. However, as the concentration of $PLGA_3$-b-PEG_7-b-$PLGA_3$ increases to $c_{cp} = 20\%$, the E, L, and G beads exhibit the widest spatial distribution, corresponding to a columnar structure. When c_{cp} further increases from 30% to 40%, the distribution of the E, L, and G beads becomes narrower again, with the E beads positioned on both sides of the L and G beads, which is characteristic of a lamellar structure, Bänsch et al. [59].

Figure 3 demonstrates that the micellization process of $PLGA_3$-b-PEG_7-b-$PLGA_3$ in aqueous solution follows a mechanism similar to that observed for most other polymeric micelles, Yang et al. [15], Wang et al. [10]. Having confirmed that the PLGA-b-PEG-b-PLGA copolymers form micelles in aqueous solution, we next investigate the effects of the copolymer concentration and composition on the morphologies structures of the micelle and to obtain a clearer perspective, we made transversal cuts of each structure, and these can be found in the Supplementary Material (Supplementary Figure S1). To assess whether the system reaches equilibrium, the time evolution of the radial distribution functions for the PLGA-b-PEG-b-PLGA copolymer beads was analyzed. Figure 4 shows that at the initial state $t = 0$, the PLGA-b-PEG-b-PLGA copolymers and water are randomly mixed. The corresponding curve exhibits a low peak at $r < 1$, indicating weak interactions between the $PLGA_3$-b-PEG_7-b-$PLGA_3$ beads. As time evolution increases due to the significantly aggregate, the width and height of the peak exhibit an increase. And at the final state ($t = 4 \times 10^5$), the

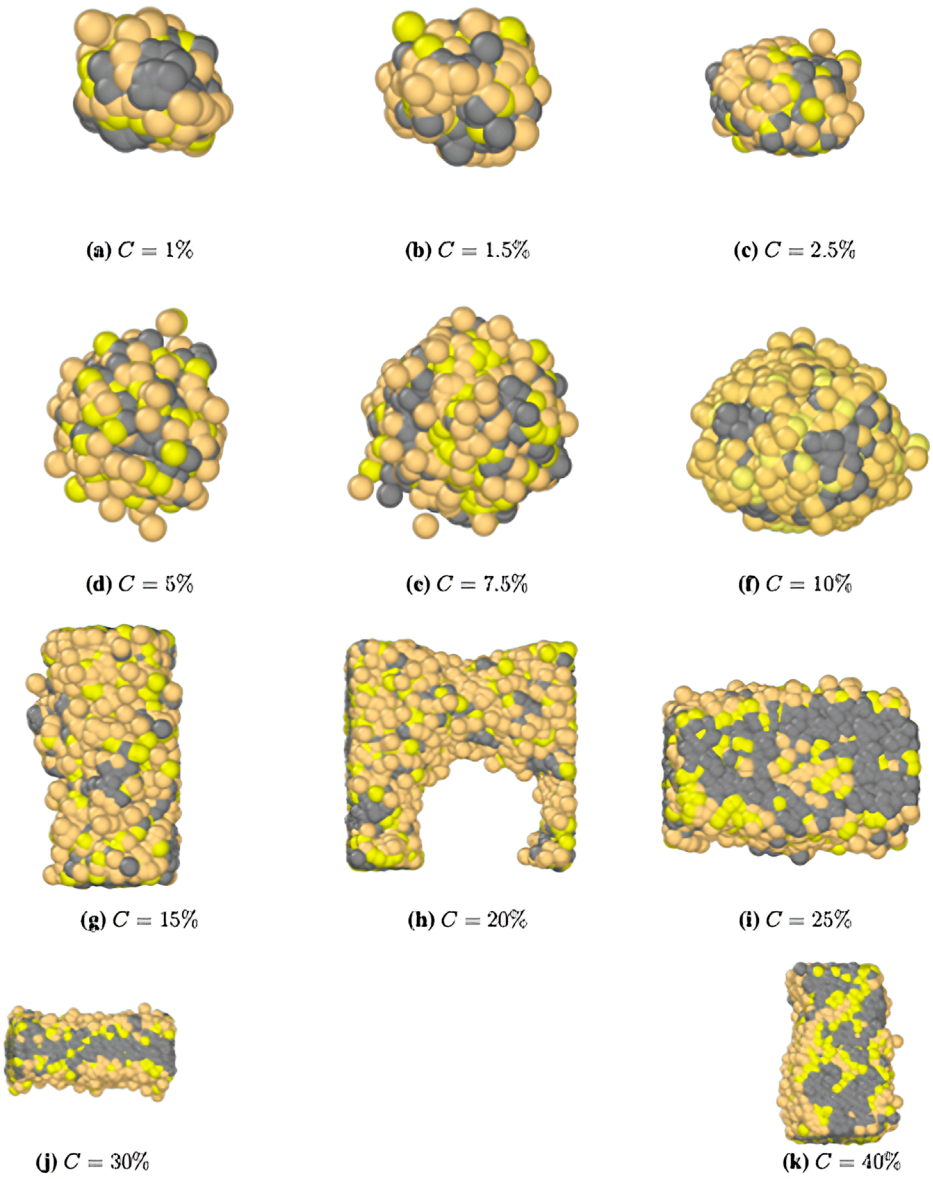

FIGURE 3
Representative morphology snapshots of the $PLGA_3$-b-PEG_7-b-$PLGA_3$ system in their final state: **(a)** C = 1%, **(b)** C = 1.5%, **(c)** C = 2.5%, **(d)** C = 5%, **(e)** C = 7.5%, **(f)** C = 10%, **(g)** C = 15%, **(h)** C = 20%, **(i)** C = 25%, **(j)** C = 30%, **(k)** C = 40%.

width and height of the peak exhibit almost no change, which indicates that the system has reached equilibrium. To obtain more quantitative insights, we plotted the radius of gyration as a function of concentration, as shown in Supplementary Figure S2 of the Supplementary Material. As shown in Supplementary Figure S2, the radius of gyration increases with concentration, confirming that aggregation is favorable, promoting micelle fusion and structural deformation when the concentrations increases from 15%.

Our findings align with the results reported by Wang Wang et al. [10], who reported similar effects of copolymer concentration on micelle morphology. Specifically, at concentrations below 10%, the micelles formed core-shell spherical structures, while at higher concentrations, they transitioned into onionlike, columnar, and lamellar structures. These findings are consistent with experimental reports of similar micelle size trends with increasing copolymer concentration Khorshid et al. [12], and also with the report by Shen Shen et al. [60], that demonstrates comparable structural transitions in PEG-PLGA micelles as the copolymer concentration increased.

Our results show that the G bead behaves like de hidrophilic core sorrounded by the E bead and finally the hidrophobic core L. With the findings of our study we show that this given difference is due to the theory used to calculate the interaction parameters, Wang et al. [10] used the Hildebrand theory, Hildebrand [61], while we used the COSMO methodology, Mullins et al. [53]. Table 3 highlights the differences between our parameters and those reported by Wang. Our model offers a more detailed representation by calculating energy interactions at the molecular level, whereas Hildebrand theory can introduce errors when estimating cohesive

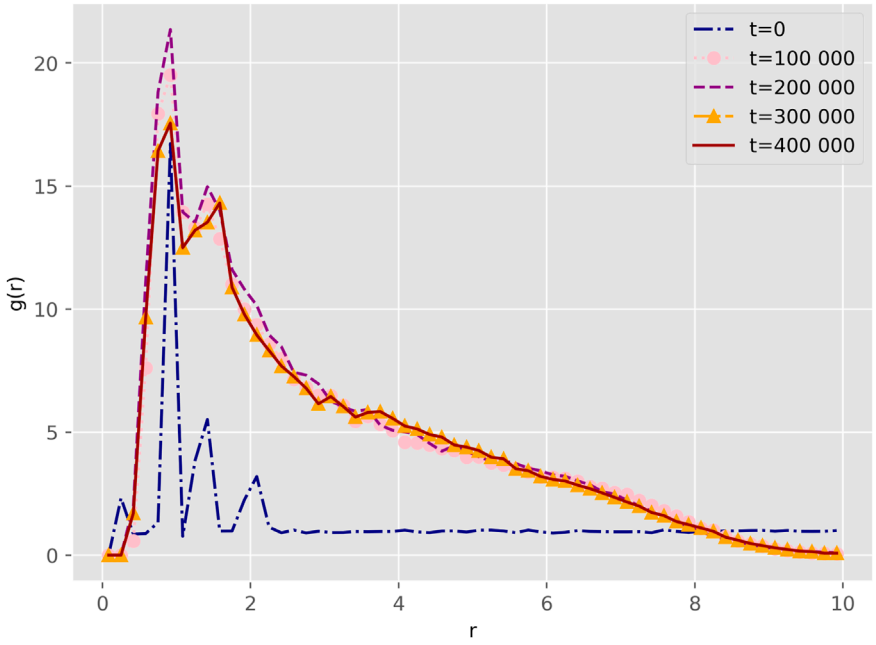

FIGURE 4
Radial distribution functions between beads of the $PLGA_3 - b - PEG_7 - b - PLGA_3$ micelles at different simulation times.

TABLE 3 Interaction parameters for the conservative force.

Species	a_{ij}	a_{ijWang}
L-G	90.37	78.04
L-E	86.65	82.96
L-W	104.07	161.00
E-G	91.13	81.76
E-W	90.04	114.00
G-W	84.07	149.30

energy Ovejero et al. [62]. Moreover, a key limitation of the Hildebrand solubility parameter is its applicability only to non-polar or weakly polar systems. Since it primarily accounts for dispersion forces, it neglects important dipole–dipole and hydrogen bonding interactions, which are essential in polar solvents and polymer systems. As a result, it may lead to inaccurate solubility predictions in systems with strong intermolecular forces, Barton [63], Venkatram et al. [64].

4 Discussion

In this study, we demonstrated that the coarse-graining method significantly influences the calculation of interaction parameters, which in turn affect the chemical behavior of the system. Methods such as COSMO and COSMO-RS have proven to be superior approaches for performing bottom-up parameterization. Polymeric micelles formed by PLGA-b-PEG-b-PLGA copolymers were investigated using Dissipative Particle Dynamics (DPD) simulations. The resulting morphologies and structures were found to depend on molecular parameters, particularly the copolymer concentration and composition.

As the PLGA-b-PEG-b-PLGA concentration increases from c_{cp} = 2.5% to 40%, the micellar structures undergo a morphological transition from spherical (core–shell) to onion-like (core–middle layer–shell), and eventually to columnar and lamellar structures. The onion-like structures consist of a hydrophilic PEG core, a hydrophobic PLGA middle layer, and a hydrophilic PEG shell. Our results reveal that the micelle structures and morphologies are highly dependent on the concentration of the PLGA-b-PEG-b-PLGA copolymer making it an excellent candidate for drug loaded micelles. From a practical point of view, a design rule can be established as follows: the relevant regime for *in vivo* applications corresponds to the copolymer concentration window where spherical or short wormlike micelles are stable, from C = 1.5% to C = 15%.

Data availability statement

The raw data supporting the conclusions of this article will be made available by the authors, without undue reservation.

Author contributions

AC-C: Conceptualization, Investigation, Validation, Visualization, Writing – original draft, Writing – review and editing. MC-C: Investigation, Visualization, Writing – review and editing.

IS-H: Conceptualization, Funding acquisition, Supervision, Writing – review and editing.

Funding

The author(s) declare that financial support was received for the research and/or publication of this article. A.AC-C. acknowledges CONAHCYT for supporting the scholarship CVU: 1184262. M.A. C-C acknowledges CONAHCYT for supporting the scholarship CVU: 1183460. A.AC-C. appreciates the technical support of Alejandro de León Cuevas, Alejandro Ávalos and Luis Alberto Aguilar Bautista from Laboratorio Nacional de Visualización Científica Avanzada (LAVIS-UNAM). A. A. Coreno-Cortés thanks Dr. Rodolfo Gómez Balderas and Dra. Roxana Mitzaye del Castillo Vazquez for their technical support. IS-H. acknowledges UMDI-J-FC UNAM for partial financial support under grant number 115377. IS-H. is grateful to LANCAD-UNAM-DGTIC-276.

Conflict of interest

The authors declare that the research was conducted in the absence of any commercial or financial relationships that could be construed as a potential conflict of interest.

Generative AI statement

The author(s) declare that no Generative AI was used in the creation of this manuscript.

Any alternative text (alt text) provided alongside figures in this article has been generated by Frontiers with the support of artificial intelligence and reasonable efforts have been made to ensure accuracy, including review by the authors wherever possible. If you identify any issues, please contact us.

Publisher's note

Supplementary material

The Supplementary Material for this article can be found online at: https://www.frontiersin.org/articles/10.3389/fphy.2025.1694078/full#supplementary-material

References

1. Cabral H, Miyata K, Osada K, Kataoka K. enBlock copolymer micelles in nanomedicine applications. *Chem Rev* (2018) 118:6844–92. doi:10.1021/acs.chemrev.8b00199

2. Hossen S, Hossain MK, Basher M, Mia M, Rahman M, Uddin MJ. Smart nanocarrier-based drug delivery systems for cancer therapy and toxicity studies: a review. *J Adv Res* (2019) 15:1–18. doi:10.1016/j.jare.2018.06.005

3. Fukushima K. enBiodegradable functional biomaterials exploiting substituted trimethylene carbonates and organocatalytic transesterification. *Polym J* (2016) 48:1103–14. doi:10.1038/pj.2016.80

4. Liao H, Gao Y, Lian C, Zhang Y, Wang B, Yang Y, et al. enOral absorption and lymphatic transport of baicalein following drug–phospholipid complex incorporation in self-microemulsifying drug delivery systems. *Int J Nanomedicine* (2019) 14:7291–306. doi:10.2147/IJN.S214883

5. Zhang S, Qian X, Zhang D, Zhu J, Wu Y, Guo Y, et al. enIn vitro anticancer efficacy by magnetic targeted nanocarrier with local delivery of paclitaxel. *Chem Res Chin Universities* (2016) 32:149–54. doi:10.1007/s40242-015-5115-1

6. Zhang K, Tang X, Zhang J, Lu W, Lin X, Zhang Y, et al. PEG–PLGA copolymers: their structure and structure-influenced drug delivery applications. *J Controlled Release* (2014) 183:77–86. doi:10.1016/j.jconrel.2014.03.026

7. Yan J, Facal Marina P, Blencowe A. enInfluence of polymerisation conditions on the kinetics of poly(lactic-*co* -glycolic acid)- *b* -poly(ethylene glycol)- *b* -poly(lactic-*co* -glycolic acid) triblock synthesis and the occurrence of transesterification side reactions. *Polym Chem* (2023) 14:2229–37. doi:10.1039/D3PY00139C

8. Yu L, Ci T, Zhou S, Zeng W, Ding J. The thermogelling PLGA–PEG–PLGA block copolymer as a sustained release matrix of doxorubicin. *Biomater Sci* (2013) 1:411. doi:10.1039/c2bm00159d

9. Chen X, Chen J, Li B, Yang X, Zeng R, Liu Y, et al. enPLGA-PEG-PLGA triblock copolymeric micelles as oral drug delivery system: *in vitro* drug release and *in vivo* pharmacokinetics assessment. *J Colloid Interf Sci* (2017) 490:542–52. doi:10.1016/j.jcis.2016.11.089

10. Wang M, Lin Y, Gao J, Liu D. enDPD simulations on morphologies and structures of blank PLGA-*b* -PEG-*b* -PLGA polymeric micelles and docetaxel-loaded PLGA-*b* -PEG-*b* -PLGA polymeric micelles. *RSC Adv* (2022) 12:12078–88. doi:10.1039/D2RA00940D

11. Chang G, Li C, Lu W, Ding J. en*N* -Boc-Histidine-Capped PLGA-PEG-PLGA as a smart polymer for drug delivery sensitive to tumor extracellular pH. *Macromolecular Biosci* (2010) 10:1248–56. doi:10.1002/mabi.201000117

12. Khorshid NK, Zhu K, Knudsen KD, Bekhradnia S, Sande SA, Nyström B. enNovel structural changes during temperature-induced self-assembling and gelation of PLGA-PEG-PLGA triblock copolymer in aqueous solutions. *Macromolecular Biosci* (2016) 16:1838–52. doi:10.1002/mabi.201600277

13. Hoogerbrugge PJ, Koelman JMVA. Simulating microscopic hydrodynamic phenomena with dissipative particle dynamics. *Europhysics Lett (Epl)* (1992) 19:155–60. doi:10.1209/0295-5075/19/3/001

14. Groot R, Rabone K. enMesoscopic simulation of cell membrane damage, morphology change and rupture by nonionic surfactants. *Biophysical J* (2001) 81:725–36. doi:10.1016/S0006-3495(01)75737-2

15. Yang Z, Zhao H, Wang D, Yin L, Cai K, Lin Z, et al. enDPD simulations on mixed polymeric DOX-Loaded micelles assembled from PCL-SS-PPEGMA/PDEA–PPEGMA and their dual pH/reduction-responsive release. *Phys Chem Chem Phys* (2021) 23:19011–21. doi:10.1039/D1CP02750F

16. Cooke IR, Kremer K, Deserno M. Tunable generic model for fluid bilayer membranes. *Phys Rev E* (2005) 72:011506. doi:10.1103/PhysRevE.72.011506

17. Cooke IR, Deserno M. Solvent-free model for self-assembling fluid bilayer membranes: stabilization of the fluid phase based on broad attractive tail potentials. *The J Chem Phys* (2005) 123:224710. doi:10.1063/1.2135785

18. Elezgaray J, Laguerre M. enA systematic method to derive force fields for coarse-grained simulations of phospholipids. *Computer Phys Commun* (2006) 175:264–8. doi:10.1016/j.cpc.2006.01.009

19. Shelley JC, Shelley MY, Reeder RC, Bandyopadhyay S, Klein ML. enA coarse grain model for phospholipid simulations. *The J Phys Chem B* (2001) 105:4464–70. doi:10.1021/jp010238p

20. Marrink SJ, Risselada HJ, Yefimov S, Tieleman DP, De Vries AH. enThe MARTINI force field: coarse grained model for biomolecular simulations. *The J Phys Chem B* (2007) 111:7812–24. doi:10.1021/jp071097f

21. Nivón-Ramírez D, Reyes-García LI, Oviedo-Roa R, Gómez-Balderas R, Zuriaga-Monroy C, Martínez-Magadán J-M. Critical micelle concentration of SDS through DPD simulations using COSMO-RS–based interaction parameters, the thermal effects. *Colloids Surf A: Physicochemical Eng Aspects* (2022) 645:128867. doi:10.1016/j.colsurfa.2022.12867

22. Shimoyama Y, Iwai Y. enDevelopment of activity coefficient model based on COSMO method for prediction of solubilities of solid solutes in supercritical carbon dioxide. *The J Supercrit Fluids* (2009) 50:210–7. doi:10.1016/j.supflu.2009.06.004

23. Grensemann H, Gmehling J. enPerformance of a conductor-like screening model for real solvents model in Comparison to Classical Group contribution methods. *Ind and Eng Chem Res* (2005) 44:1610–24. doi:10.1021/ie049139z

24. Merker T, Hsieh C, Lin S, Hasse H, Vrabec J. enFluid-phase coexistence for the oxidation of span style=font-variant:small-caps. *AIChE J* (2013) 59:2236–50. doi:10.1002/aic.13986

25. Gaube J, Fredenslund enA, Gmehling J, Rasmussen P. Vapor-Liquid equilibria using UNIFAC a group-contribution method. *Berichte der Bunsengesellschaft für physikalische Chem* (1978) 82:551. doi:10.1002/bbpc.197800104

26. Groot RD, Warren PB. enDissipative particle dynamics: bridging the gap between atomistic and mesoscopic simulation. *The J Chem Phys* (1997) 107:4423–35. doi:10.1063/1.44784

27. Groot RD. *Applications of dissipative particle dynamics*. Berlin Heidelberg: Springer (2004). p. 5–38. doi:10.1007/978-3-540-39895-0_1

28. Oviedo-Roa R, Martínez-Magadán JM, Muñoz-Colunga A, Gómez-Balderas R, Pons-Jiménez M, Zamudio-Rivera LS. Critical micelle concentration of an ammonium salt through dpd simulations using cosmo-rs–based interaction parameters. *AIChE J* (2013) 59:4413–23. doi:10.1002/aic.14158

29. Nivón-Ramírez D, Reyes-García LI, Oviedo-Roa R, Gómez-Balderas R, Zuriaga-Monroy C, Martínez-Magadán J-M. Critical micelle concentration of sds through dpd simulations using cosmo-rs–based interaction parameters, the thermal effects. *Colloids Surf A: Physicochemical Eng Aspects* (2022) 645:128867. doi:10.1016/j.colsurfa.2022.128867

30. Alasiri H, Chapman WG. Dissipative particle dynamics (dpd) study of the interfacial tension for alkane/water systems by using cosmo-rs to calculate interaction parameters. *J Mol Liquids* (2017) 246:131–9. doi:10.1016/j.molliq.2017.09.056

31. Saathoff J. Effectively parameterizing dissipative particle dynamics using cosmo-sac: a partition coefficient study. *The J Chem Phys* (2018) 148:154102. doi:10.1063/1.5019952

32. Maiti A, McGrother S. enBead–bead interaction parameters in dissipative particle dynamics: relation to bead-size, solubility parameter, and surface tension. *The J Chem Phys* (2004) 120:1594–601. doi:10.1063/1.163294

33. Rajkamal N, Vedantam S. Dissipative particle dynamics study of intracellular delivery in capsules deformed by microfluidic constriction channels. *Int J Comput Methods Eng Sci Mech* (2025) 26:56–75. doi:10.1080/15502287.2024.2447309

34. Wang M, Lin Y, Gao J, Liu D. Dpd simulations on morphologies and structures of blank plga-b-peg-b-plga polymeric micelles and docetaxel-loaded plga-b-peg-b-plga polymeric micelles. *RSC Adv* (2022) 12:12078–88. doi:10.1039/d2ra00940d

35. Lee S, Kang S, Kim WJ. Targeted protein degradation in cancer therapy *via* hydrophobic polymer-tagged nanoparticles. *ACS Nano* (2025) 19:7742–54. doi:10.1021/acsnano.4c12747

36. Klamt A, Eckert F. Cosmo-rs: a novel and efficient method for the *a priori* prediction of thermophysical data of liquids. *Fluid Phase Equilibria* (2000) 172:43–72. doi:10.1016/s0378-3812(00)00357-5

37. Klamt A. The cosmo and cosmo-rs solvation models. *WIREs Comput Mol Sci* (2011) 1:699–709. doi:10.1002/wcms.56

38. Klamt A. The cosmo and cosmo-rs solvation models. *WIREs Comput Mol Sci* (2017) 8:e1338. doi:10.1002/wcms.1338

39. Schäfer A, Horn H, Ahlrichs R. Fully optimized contracted gaussian basis sets for atoms li to kr. *The J Chem Phys* (1992) 97:2571–7. doi:10.1063/1.463096

40. Schäfer A, Huber C, Ahlrichs R. Fully optimized contracted gaussian basis sets of triple zeta valence quality for atoms li to kr. *The J Chem Phys* (1994) 100:5829–35. doi:10.1063/1.467146

41. Ahlrichs R, Bär M, Häser M, Horn H, Kölmel C. Electronic structure calculations on workstation computers: the program system turbomole. *Chem Phys Lett* (1989) 162:165–9. doi:10.1016/0009-2614(89)85118-8

42. Klamt A, Schüürmann G. Cosmo: a new approach to dielectric screening in solvents with explicit expressions for the screening energy and its gradient. *J Chem Soc Perkin Trans* (1993) 2:799–805doi. doi:10.1039/p29930000799

43. Diedenhofen M, Klamt A. Cosmo-rs as a tool for property prediction of il mixtures—a review. *Fluid Phase Equilibria* (2010) 294:31–8. doi:10.1016/j.fluid.2010.02.002

44. Xu RL, Winnik* MA, Hallett FR, Riess G, Croucher MD. Light scattering study of the association behavior of styrene-ethylene oxide block copolymers in aqueous solution. *Macromolecules* (1991) 24:87–93. doi:10.1021/ma00001a014

45. Groot RD, Warren PB. Dissipative particle dynamics: bridging the gap between atomistic and mesoscopic simulation. *The J Chem Phys* (1997) 107:4423–35. doi:10.1063/1.474784

46. Groot R, Rabone K. Mesoscopic simulation of cell membrane damage, morphology change and rupture by nonionic surfactants. *Biophysical J* (2001) 81:725–36. doi:10.1016/s0006-3495(01)75737-2

47. Maiti A, McGrother S. Bead–bead interaction parameters in dissipative particle dynamics: relation to bead-size, solubility parameter, and surface tension. *The J Chem Phys* (2004) 120:1594–601. doi:10.1063/1.1630294

48. Khedr A, Striolo A. Dpd parameters estimation for simultaneously simulating water–oil interfaces and aqueous nonionic surfactants. *J Chem Theor Comput* (2018) 14:6460–71. doi:10.1021/acs.jctc.8b00476

49. Kuru MM, Dalgakiran EA, Kacar G. Investigation of morphology, micelle properties, drug encapsulation and release behavior of self-assembled peg-pla-peg block copolymers: a coarse-grained molecular simulations study. *Colloids Surf A: Physicochemical Eng Aspects* (2021) 629:127445. doi:10.1016/j.colsurfa.2021.127445

50. Yildiz M, Kacar G. Investigation of ibuprofen loading in peg–plga–peg micelles by coarse-grained dpd simulations. *MRS Adv* (2021) 6:689–94. doi:10.1557/s43580-021-00073-6

51. Scheffczyk J, Schäfer P, Fleitmann L, Thien J, Redepenning C, Leonhard K, et al. Cosmo-campd: a framework for integrated design of molecules and processes based on cosmo-rs. *Mol Syst Des and Eng* (2018) 3:645–57. doi:10.1039/c7me00125h

52. Klamt A, Eckert F, Hornig M. *J Computer-Aided Mol Des* (2001) 15:355–65. doi:10.1023/a1011111506388

53. Mullins E, Oldland R, Liu YA, Wang S, Sandler SI, Chen C-C, et al. enSigma-Profile database for using COSMO-Based thermodynamic methods. *Ind and Eng Chem Res* (2006) 45:4389–415. doi:10.1021/ie060370h

54. Al-Jabri M, Rodgers T. The effect of changing the molecular structure of the surfactant on the dissolution of lamellar phases. *J Colloid Interf Sci* (2023) 643:9–16. doi:10.1016/j.jcis.2023.03.205

55. Seaton MA, Anderson RL, Metz S, Smith W. DL_MESO: highly scalable mesoscale simulations. *Mol Simulation* (2013) 39:796–821. doi:10.1080/08927022.2013.772297

56. Guo XD, Tan JPK, Zhang LJ, Khan M, Liu SQ, Yang YY, et al. enPhase behavior study of paclitaxel loaded amphiphilic copolymer in two solvents by dissipative particle dynamics simulations. *Chem Phys Lett* (2009) 473:336–42. doi:10.1016/j.cplett.2009.04.009

57. Yu L, Zhang Z, Zhang H, Ding J. enMixing a sol and a precipitate of block copolymers with different block ratios leads to an injectable hydrogel. *Biomacromolecules* (2009) 10:1547–53. doi:10.1021/bm900145g

58. Guo S-H, Yu X-K, Zhu Y-L, Zhang L-L, Huang Y-N. enControlled release mechanism of drugs from onion-like dendrimersomes: insight from dissipative particle dynamics simulations. *Phys Chem Chem Phys* (2025) 27:9087–94. doi:10.1039/D4CP04780J

59. Bänsch F, Steinbeck C, Zielesny A. Notes on molecular fragmentation and parameter settings for a dissipative particle dynamics study of a C10E4/water mixture with lamellar bilayer formation. *J Cheminformatics* (2023) 15:23. doi:10.1186/s13321-023-00697-w

60. Shen L, Amatulli G, Sethi T, Raymond P, Domisch S. Estimating nitrogen and phosphorus concentrations in streams and rivers across the Contiguous United States (2019). doi:10.1594/PANGAEA.899168

61. Hildebrand JH. A critique of the theory of solubility of non-electrolytes. *Chem Rev* (1949) 44:37–45. doi:10.1021/cr60137a003

62. Ovejero G, Romero M, Díez E, Díaz I. enThermodynamic interactions of three SBS (styrene–butadiene–styrene) triblock copolymers with different solvents, by means of intrinsic viscosity measurements. *Eur Polym J* (2010) 46:2261–8. doi:10.1016/j.eurpolymj.2010.10.016

63. Barton AF. *enCRC handbook of solubility parameters and other cohesion parameters: second edition*. 2 edn. New York: Routledge (2017). doi:10.1201/9781315140575

64. Venkatram S, Kim C, Chandrasekaran A, Ramprasad R. enCritical assessment of the hildebrand and hansen solubility parameters for polymers. *J Chem Inf Model* (2019) 59:4188–94. doi:10.1021/acs.jcim.9b00656